Reliable Integer Ambiguity Resolution: Multi-Frequency Code Carrier Linear Combinations and Statistical A Priori Knowledge of Attitude

P. HENKEL
Technische Universität München (TUM), Munich, Germany

C. GÜNTHER
German Aerospace Center (DLR), Oberpfaffenhofen, Germany

Received February 2011; Revised December 2011

ABSTRACT: *This paper provides two methods to improve the reliability of carrier phase integer ambiguity resolution: The first one is a group of multi-frequency linear combinations that include both code and carrier phase measurements, and allow an arbitrary scaling of the geometry, an arbitrary scaling of the ionospheric delay, and any preferred wavelength. The maximization of the ambiguity discrimination results in combinations with a wavelength of several meters and a noise level of a few centimeters. These combinations could be beneficial for both Real-Time Kinematics (RTK) and Precise Point Positioning (PPP).*

The second method incorporates some statistical a priori knowledge of attitude into the actual fixing. The a priori knowledge includes the length and direction of the baseline between two receivers and is given either as a uniform or Gaussian distribution. It enables a substantial reduction of the search space volume but also ensures a large robustness over errors in the a priori information.

Both methods improve the accuracy of the float solution, which motivates a simple rounding for ambiguity fixing. A method is described, which enables an efficient computation of its success rate with a few integral transformations.

INTRODUCTION

Real-time kinematic (RTK) positioning uses double difference carrier phase measurements. The double differencing eliminates both receiver and satellite biases and clock offsets, which simplifies the resolution of the carrier phase integer ambiguities. Currently, there exist mainly three error sources that limit the reliability of integer resolution: First, there is the double difference ionospheric delay, which only cancels for short baselines. Secondly, the double difference tropospheric delay is often neglected, which introduces some errors especially if there is a significant difference in the height between both receivers. The third and probably most challenging error source is multipath.

Figure 1 shows the probability of wrong fixing for widelane ambiguity resolution with bootstrapping [1] as a function of the baseline length. We can observe a substantial increase in the failure rate if there is an ionospheric gradient of 1 mm/km between both receivers. It causes a double difference ionospheric delay which occurs as a bias in the ambiguity resolution [2]. The probability of wrong fixings are shown in Figure 1 for bootstrapping with and without integer decorrelation, where the latter one enables a certain improvement over the first one. The float ambiguities, the baseline and the tropospheric zenith delay were estimated from two dual frequency E1-E5 combinations of Galileo double difference measurements: the classical ionosphere-free code only combination and the classical phase-only widelane combination. The latter one increases the wavelength by a factor of 4.16 but also amplifies the ionospheric delay by a factor 1.32. Both combinations were smoothed over 60 s with an ionosphere-free phase only combination. The satellite geometry was computed from the Galileo Walker constellation as seen from our institute. An epoch with eight visible satellites was selected.

Obviously, the failure rates significantly increase if the ionospheric gradient rises to 5 mm/km, which is still two orders of magnitude below the largest ionospheric gradient that has been observed so far. This is the motivation for the derivation and analysis of a new set of linear combinations, that enable an arbitrary scaling of the ionospheric delay and any preferred wavelength.

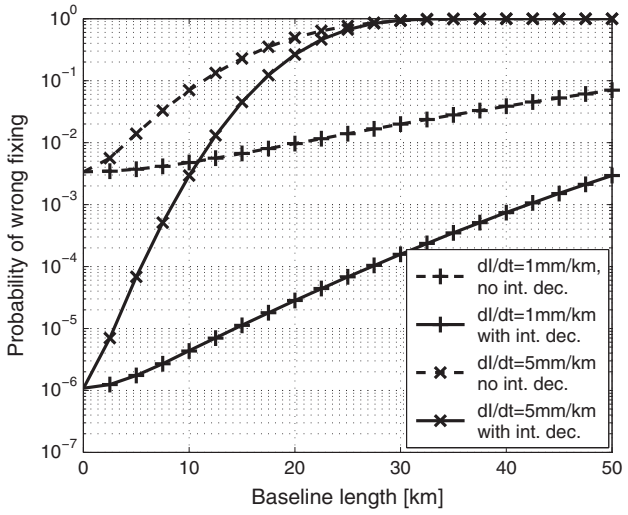

Fig. 1–Reliability of widelane ambiguity resolution with double difference measurements

MULTI-FREQUENCY MIXED CODE CARRIER LINEAR COMBINATIONS

Multi-frequency linear combinations are an efficient approach to improve the reliability of carrier phase integer ambiguity resolution. The linear combinations enable a significant suppression of the ionospheric delay and an increase in the wavelength, while the range information is kept. A systematic search of all possible dual frequency phase-only widelane combinations has been performed by Cocard and Geiger in [3] and by Collins in [4]. An L1-L2 linear combination with a wavelength of 14.65 m was found. However, the combination also amplifies the ionospheric delay by more than 25 dB. The generalization to measurements on three and more frequencies enables much more attractive linear combinations as shown by Henkel and Günther in [5], by Wübbena in [6], or by Richert and El-Sheimy in [7]. For example, a Galileo triple frequency E1-E5a-E5b linear combination with a wavelength of 3.285 m suppresses the ionospheric delay by 17 dB. However, a complete elimination of the ionosphere is not achievable with phase-only widelane combinations. Therefore, the authors suggested the inclusion of code measurements in the linear combination in [8]. The ambiguity discrimination was introduced as an optimization criterion for the combinations: It was defined as the ratio between the wavelength and twice the standard deviation of noise, which shall be maximized. The code measurements relax the integer constraint and enable the computation of a dual frequency geometry-preserving, ionosphere-free linear combination with a wavelength of 3.285 m and a noise level of a few centimeters. In [9], Henkel, Gomez and Günther presented multi-frequency code carrier linear combinations including the Galileo signals on E1, E5 and E6. In [10], Henkel gave a detailed derivation of code carrier combinations of maximum discrimination for an arbitrary number of frequencies.

In this section, the class of linear code carrier combinations is further generalized such that an arbitrary scaling of the geometry, an arbitrary scaling of the ionospheric delay, and any preferred wavelength are feasible as proposed by the authors in [11–13, 25]. The code measurements from satellite k observed at user u on frequency m are modeled as

$$\begin{aligned}\rho^k_{u,m} = &\left\|x_u - x^k\right\| + \left(e^k_u\right)^T \delta x^k + c\left(\delta\tau_u - \delta\tau^k\right) \\ &+T^k_u + q^2_{1m} I'^k_{u,1} + q^3_{1m} I''^k_{u,1} + b_{\rho_{u,m}} + b_{\rho^k_m} \\ &+o_{\rho^k_{u,m}} + \epsilon_{\rho^k_{u,m}}\end{aligned} \tag{1}$$

with user position x_u, satellite position x^k, unit vector e^k_u pointing from the satellite to the receiver, satellite position error δx^k due to imperfect knowledge of the orbit, receiver clock offset $\delta\tau_u$, satellite clock offset $\delta\tau^k$, speed of light c, tropospheric delay T^k_u, ratio of frequencies $q_{1m} = f_1/f_m$, first and second order ionospheric delays $\left\{I'^k_{u,1}, I''^k_{u,1}\right\}$ on L1/E1, receiver code bias $b_{\rho_{u,m}}$, satellite code bias $b_{\rho^k_m}$, delay $o_{\rho^k_{u,m}}$ due to code multipath, and code noise $\epsilon_{\rho^k_{u,m}}$. A similar model is used for the carrier phase measurements:

$$\begin{aligned}\lambda_m \phi^k_{u,m} = &\left\|x_u - x^k\right\| + \left(e^k_u\right)^T \delta x^k + c\left(\delta\tau_u - \delta\tau^k\right) \\ &+T^k_u - q^2_{1m} I'^k_u - \frac{1}{2} q^3_{1m} I''^k_u + b_{\phi_{u,m}} + b_{\phi^k_m} \\ &+o_{\phi^k_{u,m}} + \lambda_m N^k_{u,m} + \varepsilon_{\phi^k_{u,m}}\end{aligned} \tag{2}$$

with wavelength λ_m and carrier phase integer ambiguity $N^k_{u,m}$. The code and carrier phase measurements of (1) and (2) are linearly combined in (3) with the phase weight α_m and the code weight β_m.

$$\begin{aligned}\sum_{m=1}^{M}\left(\alpha_m\lambda_m\phi^k_{u,m} + \beta_m\rho^k_{u,m}\right) = &\left(\sum_{m=1}^{M}(\alpha_m+\beta_m)\right)\cdot\left(\left\|x_u - x^k\right\| + \left(e^k_u\right)^T\delta x^k + c\left(\delta\tau_u - \delta\tau^k\right) + T^k_u\right) \\ &+\left(\sum_{m=1}^{M}(\alpha_m-\beta_m)\mathrm{q}^2_{1m}\right)\cdot I'^k_{u,1} + \left(\sum_{m=1}^{M}\left(\frac{1}{2}\alpha_m - \beta_m\right)\mathrm{q}^3_{1m}\right)\cdot \mathrm{I}''^k_{u,1} \\ &+\left(\sum_{m=1}^{M}\alpha_m\lambda_m N^k_{u,m}\right) + \left(\sum_{m=1}^{M}\alpha_m\left(b_{\phi_{u,m}} + b_{\phi^k_m}\right) + \beta_m\left(b_{\rho_{u,m}} + b_{\rho^k_m}\right)\right) \\ &+\left(\sum_{m=1}^{M}\left(\alpha_m o_{\phi^k_{u,m}} + \beta_m o_{\rho^k_{u,m}}\right)\right) + \left(\sum_{m=1}^{M}\left(\alpha_m\varepsilon_{\phi^k_{u,m}} + \beta_m\varepsilon_{\rho^k_{u,m}}\right)\right)\end{aligned} \tag{3}$$

The choice of these weights is obtained from some constraints on the geometry, ionospheric delay, combined multipath and biases, and a further optimization that shall be described later in this section. The first term on the right side of (3) describes the geometry term which can be scaled by any arbitrary value h_1, i.e.,

$$\sum_{m=1}^{M}(\alpha_m+\beta_m)=h_1 \tag{4}$$

A geometry-free combination is obtained if $h_1=0$ and a geometry-preserving one if $h_1=1$. Note that the scaling of the geometry also affects the orbital error, the clock offsets and the tropospheric delay. The first order ionospheric delay, $I'^{k}_{u,1,}$ can also be scaled by any arbitrary value h_2, i.e.,

$$\sum_{m=1}^{M}(\alpha_m-\beta_m)q_{1m}^2=h_2 \tag{5}$$

where $h_2=0$ corresponds to an ionosphere-free and $h_2=-1$ to an ionosphere-preserving combination. However, a scaling factor in between -1 and 0 could be interesting if a certain ionospheric suppression is already achieved by double differencing. In this case, (3) can be substantially simplified, i.e. the clock offsets, phase biases and code biases are eliminated by double differencing. Similarly, the second order ionospheric delay can also be scaled by any value h_3, i.e.,

$$\sum_{m=1}^{M}\left(\frac{1}{2}\alpha_m-\beta_m\right)q_{1m}^3=h_3 \tag{6}$$

The next term on the right side of (3) describes the linear combination of integer ambiguities which shall be equal to a single integer ambiguity N_u^k times the wavelength λ of the linear combination, i.e.,

$$\sum_{m=1}^{M}\alpha_m\lambda_m N_{u,m}^k=\lambda N_u^k \tag{7}$$

which can be easily solved for N_u^k:

$$N_u^k=\sum_{m=1}^{M}\underbrace{\frac{\alpha_m\lambda_m}{\lambda}}_{=j_m\in\mathbb{Z}}N_{u,m}^k \tag{8}$$

As $N_{u,m}^k$ is an unknown integer, j_m must be an integer to obtain an integer N_u^k for any $N_{u,m}^k$. Rearranging (8) gives the phase weight

$$\alpha_m=\frac{j_m\lambda}{\lambda_m} \tag{9}$$

which depends on the integer weight j_m and the wavelength λ of the linear combination. The next term on the right side of (3) includes the linear combination of code and carrier phase biases. It can also be considered in the combination design, e.g., by a pre-defined upper bound, b_{max}, on the worst-case combined bias, i.e.,

$$\sum_{m=1}^{M}|\alpha_m|\left(\left|b_{\phi_{u,m}}\right|+\left|b_{\phi_m^k}\right|\right)+|\beta_m|\left(\left|b_{\rho_{u,m}}\right|+\left|b_{\rho_m^k}\right|\right)\le b_{max} \tag{10}$$

which requires some assumptions on the measurement biases. The superposition of multipath delays can also be included in the combination design, e.g., by

$$\sum_{m=1}^{M}\left(|\alpha_m|\cdot\left|o_{\phi_{u,m}^k}\right|+|\beta_m|\cdot\left|o_{\rho_{u,m}^k}\right|\right)\le o_{max} \tag{11}$$

with a pre-defined upper bound, o_{max}, on the worst-case superposition of multipath delays. These could be chosen from an elevation-dependant exponential function, i.e.,

$$o_{\phi_{u,m}^k}=o_0\cdot e^{-\frac{E}{\gamma}} \tag{12}$$

with decay constant γ and elevation angle E. Finally, the last term on the right side of (3) describes the linear combination of phase and code noises. Its variance is given by

$$\sigma^2=\sum_{m=1}^{M}\left(\alpha_m^2\sigma^2_{\varepsilon_{\phi_{u,m}^k}}+\beta_m^2\sigma^2_{\varepsilon_{\rho_{u,m}^k}}\right) \tag{13}$$

and can be minimized under the consideration of all other constraints. Alternatively, the ambiguity discrimination can be maximized. It was first introduced by Henkel and Günther in [8] as

$$D=\frac{\lambda}{2\sigma} \tag{14}$$

Its maximization corresponds to the minimization of the probability of wrong fixing for a geometry-free, ionosphere-free linear combination. As this paper is focussing more on the reliability than on the accuracy, further analysis is restricted to the class of linear combinations that maximize D.

Let us start the derivation of the optimum α_m and β_m by introducing the total phase weight

$$w_\phi=\sum_{m=1}^{M}\alpha_m=\lambda\sum_{m=1}^{M}\frac{j_m}{\lambda_m} \tag{15}$$

which can be solved for the wavelength λ of the linear combination, i.e.,

$$\lambda=\frac{w_\phi}{\sum_{m=1}^{M}\frac{j_m}{\lambda_m}} \tag{16}$$

Replacing λ in (9) by (16) gives

$$\alpha_m=\frac{j_m}{\lambda_m}\lambda=\frac{j_m}{\lambda_m}\frac{1}{\sum_{m=1}^{M}\frac{j_m}{\lambda_m}}w_\phi \tag{17}$$

The constraints on the geometry and first order ionospheric delay are written in matrix–vector notation using (4), (5) and (17), i.e.,

$$\Psi_1 \begin{bmatrix} \beta_1 \\ \beta_2 \end{bmatrix} + \Psi_2 \begin{bmatrix} w_\phi \\ \beta_3 \\ \vdots \\ \beta_M \end{bmatrix} = \begin{bmatrix} h_1 \\ h_2 \end{bmatrix} \tag{18}$$

with

$$\Psi_1 = \begin{bmatrix} 1 & 1 \\ -1 & -q_{12}^2 \end{bmatrix} \tag{19}$$

and

$$\Psi_2 = \begin{bmatrix} 1 & 1 & \dots & 1 \\ \sum_{m=1}^{M} \frac{j_m}{\lambda_m} \frac{1}{\sum_{m=1}^{M} \frac{j_m}{\lambda_m}} q_{1m}^2 & -q_{13}^2 & \dots & -q_{1M}^2 \end{bmatrix} \tag{20}$$

Note that the second order ionospheric delay has not been included in (18) as it is often negligible. Eq. (18) can be solved for the code weights β_1 and β_2:

$$\begin{aligned} \begin{bmatrix} \beta_1 \\ \beta_2 \end{bmatrix} &= \Psi_1^{-1} \left(\begin{bmatrix} h_1 \\ h_2 \end{bmatrix} - \Psi_2 \begin{bmatrix} w_\phi \\ \beta_3 \\ \vdots \\ \beta_M \end{bmatrix} \right) \\ &= \begin{bmatrix} s_1 + s_2 w_\phi + \sum_{m=3}^{M} s_m \beta_m \\ t_1 + t_2 w_\phi + \sum_{m=3}^{M} t_m \beta_m \end{bmatrix} \end{aligned} \tag{21}$$

where the s_m and t_m, $m \in \{1, \dots, M\}$, are implicitly defined by the last equality. Equation (21) leaves the integer coefficients j_m, $m \geq 1$, the code weights β_m, $m \geq 3$, and the total phase weight w_ϕ as unknowns. The maximization of D over these variables shall be performed in two steps as shown in Figure 2.

First, a numerical search is performed with a maximization over j_m and, secondly, an analytical computation is performed with a maximization over w_ϕ and β_m. Equation (28) provides an expression of the ambiguity discrimination that is obtained from (14) using (16), (17), (21) and (13), and only depends on w_ϕ and β. Some abbreviations were introduced to simplify the notation:

$$\tilde{\eta}^2 = \sum_{m=1}^{M} \frac{j_m^2}{\lambda_m^2} \frac{1}{\left(\sum_{m=1}^{M} \frac{j_m}{\lambda_m} \right)^2} \sigma_{\phi_m}^2 \tag{22}$$

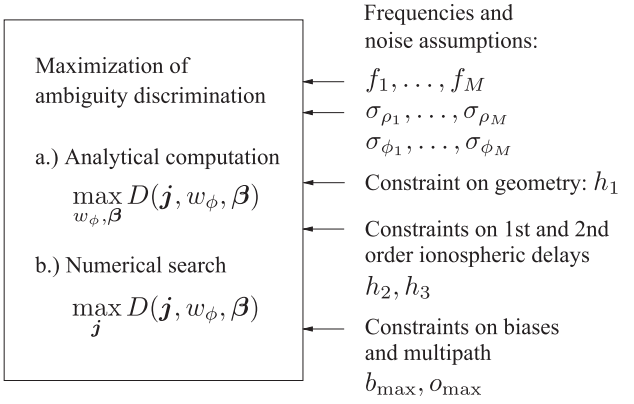

Fig. 2–Computation of multi-frequency code carrier linear combinations of maximum ambiguity discrimination

$$\Sigma = \begin{bmatrix} \sigma_{\rho_3}^2 & \dots & \sigma_{\rho_3 \rho_M} \\ \vdots & \ddots & \vdots \\ \sigma_{\rho_3 \rho_M} & \dots & \sigma_{\rho_M}^2 \end{bmatrix} \tag{23}$$

as well as $\beta = [\beta_3, \dots, \beta_M]^T$, $s = [s_3, \dots, s_M]^T$, and $t = [t_3, \dots, t_M]^T$. The maximization with respect to w_ϕ results in the constraint

$$\frac{\partial D}{\partial w_\phi} \stackrel{!}{=} 0 \tag{24}$$

and the maximization with respect to β gives

$$\frac{\partial D}{\partial \beta} \stackrel{!}{=} 0 \tag{25}$$

The latter constraint can be developed as

$$\begin{aligned} &\left(s_1 + s_2 w_\phi + s^T \beta\right) s \cdot \sigma_{\rho_1}^2 \\ &+ \left(t_1 + t_2 w_\phi + t^T \beta\right) t \cdot \sigma_{\rho_2}^2 + \Sigma \beta \\ &= \sigma_{\rho_1}^2 s \left(s_1 + s_2 w_\phi + s^T \beta\right) + \sigma_{\rho_2}^2 t \left(t_1 + t_2 w_\phi + t^T \beta\right) + \Sigma \beta \end{aligned} \tag{26}$$

$$\begin{aligned} &= \underbrace{\left[\sigma_{\rho_1}^2 s s^T + \sigma_{\rho_2}^2 t t^T + \Sigma\right]}_{A} \beta + \underbrace{\left[s_2 \sigma_{\rho_1}^2 s + t_2 \sigma_{\rho_2}^2 t\right]}_{b} w_\phi \\ &+ \underbrace{\left[s_1 \sigma_{\rho_1}^2 s + t_1 \sigma_{\rho_2}^2 t\right]}_{c} = 0 \end{aligned} \tag{27}$$

which shows a linear relationship between w_ϕ and β. Solving (27) for β yields

$$\mathrm{D}\left(\mathrm{w}_\phi, \beta\right) = \frac{\lambda}{2\sigma} = \frac{\mathrm{w}_\phi}{\sum_{\mathrm{m}=1}^{\mathrm{M}} \frac{\mathrm{j_m}}{\lambda_\mathrm{m}} 2 \sqrt{\tilde{\eta}^2 \mathrm{w}_\phi^2 + \left(\mathrm{s}_1 + \mathrm{s}_2 \mathrm{w}_\phi + \mathrm{s}^\mathrm{T} \beta\right)^2 \sigma_{\rho_1}^2 + \left(\mathrm{t}_1 + \mathrm{t}_2 \mathrm{w}_\phi + \mathrm{t}^\mathrm{T} \beta\right)^2 \sigma_{\rho_2}^2 + \beta^\mathrm{T} \Sigma \beta}} \tag{28}$$

$$\beta = -A^{-1}(c + b \cdot w_\phi) \tag{29}$$

The first constraint given by (24) can also be further developed as

$$\begin{aligned}&(s_1 + s_2 w_\phi + s^T\beta)(s_1 + s^T\beta)\sigma_{\rho_1}^2 \\ &+(t_1 + t_2 w_\phi + t^T\beta)(t_1 + t^T\beta)\sigma_{\rho_2}^2 + \beta^T\Sigma\beta = 0\end{aligned}$$

Replacing β by (29) gives

$$\begin{aligned}&(s_1 + s_2 w_\phi - s^T A^{-1}(c + b w_\phi)) \cdot (s_1 - s^T A^{-1}(c + b w_\phi)) \cdot \sigma_{\rho_1}^2 \\ &+(t_1 + t_2 w_\phi - t^T A^{-1}(c + b w_\phi)) \cdot (t_1 - t^T A^{-1}(c + b w_\phi)) \cdot \sigma_{\rho_2}^2 \\ &+(c + b w_\phi)^T (A^{-1})^T \Sigma A^{-1}(c + b w_\phi) = 0\end{aligned} \tag{30}$$

which only includes w_ϕ (and j_m, hidden in A, b, c, s and t) as unknowns. Equation (30) is a quadratic equation in w_ϕ, i.e.

$$r_0 + r_1 \cdot w_\phi + r_2 \cdot w_\phi^2 = 0 \tag{31}$$

with

$$\begin{aligned}r_0 &= (s_1 - s^T A^{-1} c)^2 \sigma_{\rho_1}^2 + (t_1 - t^T A^{-1} c)^2 \sigma_{\rho_2}^2 \\ &\quad + c^T (A^{-1})^T \Sigma A^{-1} \mathbf{c} \\ r_1 &= \big((s_1 - s^T A^{-1} c)(-s^T A^{-1} b) \\ &\quad + (s_2 - s^T A^{-1} b)(s_1 - s^T A^{-1} c)\big) \cdot \sigma_{\rho_1}^2 \\ &\quad + \big((t_1 - t^T A^{-1} c)(-t^T A^{-1} b) \\ &\quad + (t_2 - t^T A^{-1} b)(t_1 - t^T A^{-1} c)\big) \cdot \sigma_{\rho_2}^2 \\ &\quad + \Big(c^T (A^{-1})^T \Sigma \mathbf{A}^{-1} b + b^T (A^{-1})^T \Sigma A^{-1} c\Big) \\ r_2 &= (s_2 - s^T A^{-1} b)(-s^T A^{-1} b) \cdot \sigma_{\rho_1}^2 \\ &\quad + (t_2 - t^T A^{-1} b)(-t^T A^{-1} b) \cdot \sigma_{\rho_2}^2 + b^T (A^{-1})^T \Sigma A^{-1} b\end{aligned} \tag{32}$$

The last term r_2 always vanishes which can be proven by replacing A, b, c, s and t by their definitions. Thus, the optimal total phase weight is given by

$$w_{\phi_{opt}} = -\frac{r_0}{r_1} \tag{33}$$

The optimal phase and code weights α_m and β_m are then obtained from (29), (21), and (17). The α_m and β_m can be optimized for any standard deviation σ_{ρ_m}. In this paper, the σ_{ρ_m} are chosen according to the Cramer Rao bound, which is given by

$$\sigma_{\rho_m} \geq \Gamma_m = \sqrt{\frac{c^2}{\frac{C}{N_0}\, T_i \cdot \frac{\int (2\pi f)^2 |S_m(f)|^2 df}{\int |S_m(f)|^2 df}}} \tag{34}$$

with speed of light c, carrier to noise power ratio $\frac{C}{N_0}$, pre-detection integration time T_i, and power spectral density $S_m(f)$. The latter has been derived by Betz in [14] for binary offset carrier (BOC) modulated signals. Table 1 shows the Cramer Rao bounds of the wideband Galileo/ GPS signals, which are used in the following analysis.

Table 1 —Cramer Rao Bounds for $C/N_0 = 45\text{dB} - \text{Hz}$

	Signal	BW [MHz]	Γ [cm]
E1	MBOC	20	11.14
E5	AltBOC(15,10)	51	1.95
E5a	BPSK(10)	20	7.83
E5b	BPSK(10)	20	7.83
E6	BPSK(5)	20	11.36
L1	BPSK(1)	20	25.92
L2C	BPSK(1)	20	25.92
L5	BPSK(10)	20	7.83

Tables 2, 3 and 4 show the optimized dual, triple, and four frequency code carrier widelane Galileo combinations of maximum discrimination for $\sigma_\phi = 1$ mm and $\sigma_{\rho_m} = \Gamma_m$.

Table 5 includes the optimized dual and triple-frequency GPS combinations. The first line in each table represents a geometry-preserving (GP) ionosphere-free (IF) combination, followed by a GP reduced ionosphere (IR, 10 dB suppression) combination that can be used for positioning. The next linear combination is a geometry-free (GF), ionosphere-preserving (IP) one, which could be applied for the estimation of the ionospheric delay. The 4th combination is both GF and IF, which makes it a candidate for ambiguity resolution, or multipath analysis. The linear combinations are characterized by a wavelength of a few meters and a noise level of several centimeters, which results in a large ambiguity discrimination D. The GP-IF combination tends to a slightly larger D than the GF-IP one but both discriminations are large enough to enable a reliable integer ambiguity resolution if multipath and biases can be estimated. A comparison of Table 2 and Table 3 shows that the processing of the E5 signal as a single wideband signal is preferred over the processing of two sub-bands, i.e., the lower code noise of the AltBOC signal more than compensates for the slightly reduced number of degrees of freedom. The inclusion of E6 measurements further increases the ambiguity discrimination, which achieves its highest value for the E5a-E5b widelane ambiguity combination. Note also that all code coefficients, β_m, of the triple and four frequency GF-IF combinations are quite small, which indicates a large robustness over code multipath.

The fifth combination in Table 5 is a dual-frequency L1-L2 widelane combination, which can be used already with today's signals. It preserves both the geometry and ionospheric delay, and is characterized by a wavelength of 1.534 m and a noise level of two decimeters, which allows quite reliable integer ambiguity resolution over short baselines. This combination also does not include code measurements on L1, which is also advantageous with respect to multipath. An even more attractive combination would be the GP ionosphere-free one. However, the maximization of the discrimination leads to a wavelength of more than 10.14 m

Table 2 —Dual-frequency code carrier widelane Galileo combinations of maximum discrimination for $\sigma_\varphi = 1$ mm and $\sigma_{\rho_m} = \Gamma_m$

h_1	h_2	E1		E5		λ	σ	D
1	0	j_1	1	j_2	−1	3.285 m	6.5 cm	25.12
		α_1	17.2629	α_2	−13.0593			
		β_1	−0.0552	β_2	−3.1484			
1	−0.1	j_1	1	j_2	−1	3.092 m	6.1 cm	25.55
		α_1	16.2508	α_2	−12.2936			
		β_1	−0.0487	β_2	−2.9085			
0	−1	j_1	−1	j_2	1	1.938 m	4.9 cm	19.65
		α_1	−10.1831	α_2	7.7035			
		β_1	0.0737	β_2	2.4059			
0	0	j_1	−1	j_2	1	1 m	8.2 cm	6.09
		α_1	−5.2550	α_2	3.9754			
		β_1	0.7285	β_2	0.5511			
h_1	h_2	E1		E5a		λ	σ	D
1	0	j_1	1	j_2	−1	4.309 m	31.4 cm	6.87
		α_1	22.6467	α_2	−16.9115			
		β_1	−1.0227	β_2	−3.7125			

Table 3 —Triple-frequency code carrier widelane Galileo combinations of max. discrimination for $\sigma_\varphi = 1$ mm and $\sigma_{\rho_m} = \Gamma_m$

h_1	h_2	E1		E5b		E5a		λ	σ	D
1	0	j_1	1	j_2	−4	j_3	3	3.603 m	13.9 cm	12.99
		α_1	18.9326	α_2	−58.0271	α_3	42.4139			
		β_1	−0.2871	β_2	−0.9899	β_3	−1.0423			
1	−0.1	j_1	1	j_2	−4	j_3	3	3.368 m	12.7 cm	13.26
		α_1	17.6991	α_2	−54.2465	α_3	39.6505			
		β_1	−0.2499	β_2	−0.9013	β_3	−0.9519			
0	−1	j_1	−1	j_2	4	j_3	−3	2.453 m	12.3 cm	9.98
		α_1	−12.8901	α_2	39.5074	α_3	−28.8772			
		β_1	0.4477	β_2	0.9061	β_3	0.9061			
0	0	j_1	0	j_2	−1	j_3	1	1 m	0.8 cm	62.71
		α_1	0	α_2	−4.0266	α_3	3.9242			
		β_1	0.0004	β_2	0.0480	β_3	0.0540			

Table 4 —Four-frequency code carrier widelane Galileo combinations of maximum discrimination for $\sigma_\varphi = 1$ mm and $\sigma_{\rho_m} = \Gamma_m$

h_1	h_2	E1		E6		E5b		E5a		λ	σ	D
1	0	j_1	1	j_2	−3	j_3	0	j_4	2	3.998 m	6.5 cm	31.02
		α_1	21.0108	α_2	−51.1627	α_3	0	α_4	31.3798			
		β_1	−0.0239	β_2	−0.0349	β_3	−0.0824	β_4	−0.0867			
1	−0.1	j_1	1	j_2	−3	j_3	0	j_4	2	3.753 m	6.0 cm	31.22
		α_1	19.7197	α_2	−48.0187	α_3	0	α_4	29.4514			
		β_1	−0.0154	β_2	−0.0233	β_3	−0.0554	β_4	−0.0585			
0	−1	j_1	−1	j_2	4	j_3	−1	j_4	−2	2.505 m	5.1 cm	24.81
		α_1	−13.1658	α_2	42.7460	α_3	−10.0881	α_4	−19.6632			
		β_1	0.0285	β_2	0.0274	β_3	0.0576	β_4	0.0576			
0	0	j_1	0	j_2	0	j_3	−1	j_4	1	1 m	0.8 cm	64.27
		α_1	0	α_2	0	α_3	−4.0266	α_4	3.9242			
		β_1	−0.0038	β_2	0.0140	β_3	0.0429	β_4	0.0493			

and a noise level of ~ 2 m, which enables reliable ambiguity resolution but is still of little use due its large noise level. The optimization of an L1-L5 combination leads to more advantageous properties (last row in Table 5) mainly due to the lower L5 code noise.

The search of the optimal integer coefficients, j_m, was performed over $|j_m| \leq 4$, and further constrained by $\sigma < 0.4$ m to prevent combinations of extremely large wavelengths, that result in a large noise level. The wavelength of the GF, IF linear combination was set to 1 m as these types of combinations leave one degree of freedom. The discrimination is independent of λ and both the GF and IF constraints are fulfilled for any λ.

Obviously, the optimized code carrier combinations depend on the assumed/estimated code noise variances but not on the phase noise variances which dropped out in the derivation. Moreover, the scaling of all code noise variances by a common factor has no impact on the optimized combinations. This is important from a practical point of view as frequent changes of linear combinations are not desired. Our suggested combinations are advantageous both with respect to their optimized phase and code coefficients

Table 5 —Multi-frequency code carrier widelane GPS combinations of maximum discrimination for $\sigma_\varphi = 1$ mm and $\sigma_{\rho_m} = \Gamma_m$

h_1	h_2		L1		L2C		L5	λ	σ	D
1	0	j_1	1	j_2	−4	j_3	3	3.338 m	10.9 cm	15.25
		α_1	17.5420	α_2	−54.6764	α_3	39.2987			
		β_1	−0.0522	β_2	−0.0860	β_3	−1.0261			
1	−0.1	j_1	1	j_2	−4	j_3	3	3.144 m	10.0 cm	15.74
		α_1	16.5210	α_2	−51.4941	α_3	37.0114			
		β_1	−0.0445	β_2	−0.0765	β_3	−0.9173			
0	−1	j_1	−1	j_2	4	j_3	−3	1.975 m	10.1 cm	9.78
		α_1	−10.3778	α_2	32.3463	α_3	−23.2489			
		β_1	0.0988	β_2	0.0988	β_3	1.0828			
0	0	j_1	0	j_2	−1	j_3	1	1 m	1.4 cm	36.95
		α_1	0	α_2	−4.0948	α_3	3.9242			
		β_1	0.0136	β_2	0.0132	β_3	0.1438			
1	−1	j_1	1	j_2	−1			1.534 m	20.2 cm	3.79
		α_1	8.0588	α_2	−6.2796					
		β_1	0	β_2	−0.7792					
1	−1	j_1	1			j_3	−1	1.313 m	5.9 cm	11.10
		α_1	6.8974			α_3	−5.1507			
		β_1	0			β_3	−0.7468			

as well as with respect to their robustness over changes in satellite elevation, which typically affects all noise variances similarly.

RELIABLE INTEGER AMBIGUITY RESOLUTION

In this section, the linear combinations of the previous section are used for reliable integer ambiguity resolution. The following model is used for the code and carrier phase measurements from all visible satellites:

$$\Psi = H\xi + AN + \eta \tag{35}$$

where H denotes the geometry matrix, ξ includes all unknown real-valued parameters, A is the wavelength matrix, N are the integer ambiguities and $\eta \sim \mathcal{N}(0, \Sigma)$ is the white Gaussian measurement noise. Note that Ψ can either consist of uncombined code and carrier phase measurements (traditional approach), or of two optimized GP linear combinations (our approach): a code carrier combination of maximum discrimination and a code-only combination of minimum noise amplification. In both cases, the estimation of ξ can be separated from the integer ambiguity resolution by an orthogonal projection, i.e.,

$$P_H^\perp \Psi = \underbrace{P_H^\perp A}_{\bar{A}} N + P_H^\perp \eta \tag{36}$$

with $P_H^\perp = 1 - H\left(H^T\Sigma^{-1}H\right)^{-1}H^T\Sigma^{-1}$. The least-squares float ambiguity solution follows from (36) as

$$\hat{N} = \left(\bar{A}^T\Sigma^{-1}\bar{A}\right)^{-1}\bar{A}^T\Sigma^{-1}\Psi \tag{37}$$

with the covariance

$$\Sigma_{\hat{N}} = \left(\bar{A}^T\Sigma^{-1}\bar{A}\right)^{-1} \tag{38}$$

The most simple integer estimation technique is rounding of the float solution of (37). The success rate heavily depends on the conditioning of the equation system. It is characterized by the condition number which is defined as the ratio between the largest and smallest eigenvalue of $\Sigma_{\hat{N}}$. The success rate can be increased by a sequential integer estimation which also takes the correlation between the float estimates into account. It was introduced by Blewitt's bootstrapping in [1], i.e., the k-th conditional ambiguity estimate can be written as

$$\hat{N}_{k|1,\ldots,k-1} = \hat{N}_k - \sum_{j=1}^{k-1}\sigma_{\hat{N}_k\hat{N}_{j|1,\ldots,j-1}}\sigma^{-2}_{\hat{N}_{j|1,\ldots,j-1}} \cdot\left(\hat{N}_{j|1,\ldots,j-1} - [\hat{N}_{j|1,\ldots,j-1}]\right), \tag{39}$$

with the conditional variance

$$\sigma^2_{\hat{N}_{k|1,\ldots,k-1}} = \sigma^2_{\hat{N}_k} - \sum_{j=1}^{k-1}\sigma^2_{\hat{N}_k\hat{N}_{j|1,\ldots,j-1}}\sigma^{-2}_{\hat{N}_{j|1,\ldots,j-1}} \tag{40}$$

and the covariance between the unconditional and conditional float ambiguities

$$\sigma_{\hat{N}_k\hat{N}_{j|1,\ldots,j-1}} = \sigma_{\hat{N}_k\hat{N}_j} - \sum_{i=1}^{j-1}\sigma_{\hat{N}_j\hat{N}_{i|1,\ldots,i-1}} \cdot\sigma^{-2}_{\hat{N}_{i|1,\ldots,i-1}}\sigma_{\hat{N}_k\hat{N}_{i|1,\ldots,i-1}} \tag{41}$$

Clearly, both the conditional variances and the covariances depend on the order of fixings. It can be easily shown that the conditional ambiguity estimates are uncorrelated, i.e.,

$$\sigma_{\hat{N}_{k|1,\ldots,k-1},\hat{N}_{l|1,\ldots,l-1}} = 0 \quad \forall\, k \neq l \tag{42}$$

Thus, the success rate of sequential ambiguity fixing can be efficiently computed from the product of one-dimensional cumulative Gaussian distributions, i.e.,

$$P_s = \prod_{k=1}^{K}\int_{-0.5}^{+0.5}\frac{1}{\sqrt{2\pi\sigma^2_{\hat{N}_{k|1,\ldots,k-1}}}} \cdot\exp\left(-\frac{(\varepsilon_{\hat{N}_{k|1,\ldots,k-1}} - b_{\hat{N}_{k|1,\ldots,k-1}})^2}{2\sigma^2_{\hat{N}_{k|1,\ldots,k-1}}}\right)d\varepsilon_{\hat{N}_{k|1,\ldots,k-1}} \tag{43}$$

Bootstrapping as well as any other integer ambiguity resolution technique can be fully described

by so called pull-in regions [15]. A pull-in region represents the set of all float ambiguities $\hat{N}$ that are mapped to the same integer vector $\breve{N}_k$ by a map $S\left(\hat{N} \rightarrow \breve{N}_k\right)$, i.e.,

$$S_{\breve{N}_k} = \left\{\hat{N} \in \mathbb{R}^{K\times 1} \middle| \breve{N}_k = S\left(\hat{N}\right)\right\}, \quad \breve{N}_k \in \mathbb{Z}^{K\times 1} \tag{44}$$

These pull-in regions shall now be analyzed for the optimal integer least-squares estimator, which is defined as

$$\breve{N} = \arg \min_{N\in\mathbb{Z}^{K\times 1}} \left\|\hat{N} - N\right\|^2_{\Sigma^{-1}_{\hat{N}}} \tag{45}$$

with $\| x \|^2_{\Sigma^{-1}} = x^T\Sigma^{-1}x$.

Figure 3 shows these pull-in regions for a double difference carrier phase positioning over a large baseline with a good satellite geometry. Subfigure (a) refers to the estimation of the E1 integers and subfigure (b) to the widelane ambiguities. Both figures also include the error ellipses given by $\left\|\hat{N} - N\right\|^2_{\Sigma^{-1}_{\hat{N}}} = c$ with $c = 3$. Obviously, the size of the error ellipse exceeds the size of a pull-in region for uncombined measurements, which indicates a low confidence in ambiguity fixing. The multi-frequency linear combinations increase the wavelength from 19.0 cm to 3.285 m and, thereby, improve the accuracy of the float solution. This results in a shrinking of the error ellipse, whose semi-major axis becomes approximately five times smaller than the width of a pull-in region. This is another indication for extremely reliable ambiguity resolution with our linear combinations. The integer least-squares estimation can be efficiently performed with the Least-squares Ambiguity Decorrelation Adjustment (LAMBDA) method of Teunissen [16]. The size of the error ellipse in Figure 3 is typical for a long-baseline kinematic positioning with a good satellite geometry and measurements from only a few epochs.

Figure 4 shows the benefit of geometry-preserving ($h_1 = 1$), ionosphere-free ($h_2 = 0$) linear combinations for Wide-Area Real-Time Kinematics (WA-RTK).

If no linear combinations are used, the baseline (once per epoch), the integer ambiguities (using bootstrapping with integer decorrelation), the tropospheric wet zenith delay and its rate, and the ionospheric slant delays for all satellites and their rates have to be estimated from double difference measurements on at least two frequencies. Here, the wideband Galileo signals on E1 (CBOC modulation) and E5 (AltBOC modulated) were considered at a carrier to noise power ratio of 45 dB-Hz.

The small wavelength and the large number of unknown parameters result in a rather poor probability of wrong fixing, which varies between 10^{-4} and 1 depending on the satellite geometry. This is far too much for Safety-of-Life critical applications,

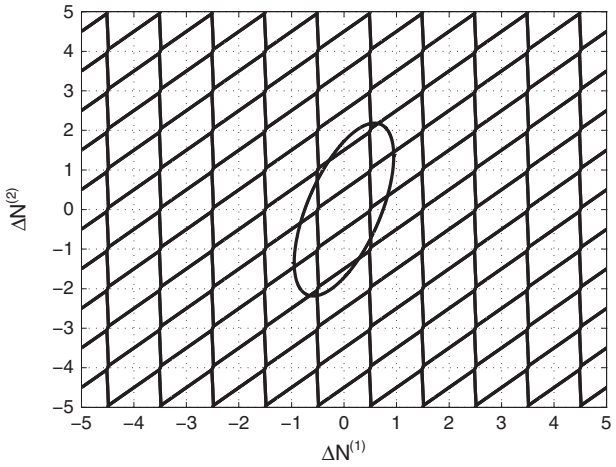

(a) E1 pull-in regions with λ = 19.0 cm

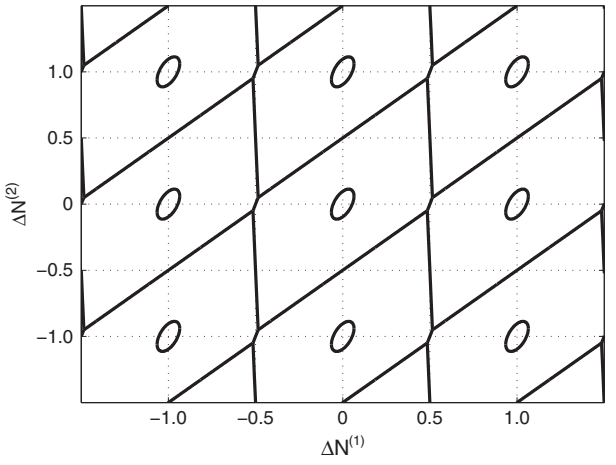

(b) Widelane pull-in regions with λ =3.285 m

Fig. 3–Reduction of ambiguity error ellipse by multi-frequency linear combinations

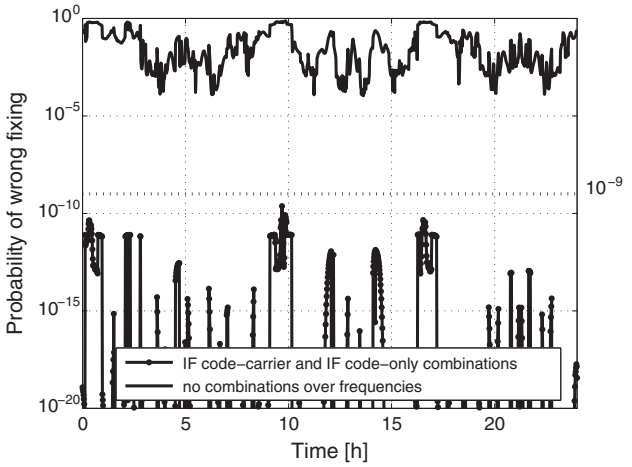

Fig. 4–Benefit of E1-E5 mixed code carrier linear combination for reliable integer ambiguity resolution

e.g., the landing of aircrafts, where a failure rate of at most 10^{-9} is required for CAT III approaches. Therefore, the use of an optimized multi-frequency code carrier combination of maximum discrimination and of a code-only combination of minimum noise amplification is analyzed. As both linear combinations are ionosphere-free, the latter two parameter sets do not have to be estimated. Figure 4 shows that the probability of wrong fixing can be reduced by several orders of magnitude due to the large wavelength of 3.285 m. The 10^{-9} requirement is fulfilled for any satellite geometry.

Figure 5 shows the benefit of a different class of linear combinations: the geometry-free ($h_1 = 0$) ones, which eliminate also the clock offsets, orbital errors and tropospheric delay. The benefit is analyzed for differential positioning with triple frequency (E1, E5a, E5b) receiver-receiver single difference measurements of 20 s. If no linear combinations are used, the carrier phase integer ambiguities, the baseline (once/ epoch), the differential receiver clock offset (once/ epoch), the ionospheric slant delays and their rates, as well as the tropospheric wet zenith delay and its rate have to be estimated.

In this traditional approach, the ambiguities were resolved sequentially according to (39) with integer decorrelation based on uncombined measurements. The use of the linear combinations significantly simplifies the ambiguity resolution: It directly provides an integer estimate that only has to be averaged over T epochs, i.e.,

$$\hat{N}^k = \frac{1}{T}\sum_{t=1}^{T}\left(\frac{1}{\lambda}\sum_{m=1}^{M}\left(\alpha_m\lambda_m\phi_m^k(t) + \beta_m\rho_m^k(t)\right)\right) \sim \mathcal{N}\left(N^k + b_u^k, \sigma^2_{\hat{N}^k}\right) \quad (46)$$

with

$$\sigma_{\hat{N}^k} = \frac{\sigma}{\lambda\sqrt{T}} = \frac{1}{2D\sqrt{T}} \quad (47)$$

and thus justifies also the maximization of the ambiguity discrimination D.

As geometry-free linear combinations imply an independant fixing of the ambiguities from all satellites, the probability of wrong fixing can be efficiently computed from

$$P_s = \prod_{k=1}^{K}\int_{-0.5}^{+0.5}\frac{1}{\sqrt{2\pi\sigma^2_{\hat{N}_k}}}\cdot e^{-\frac{\left(\varepsilon_{\hat{N}_k} - b_{\hat{N}_k}\right)^2}{2\sigma^2_{\hat{N}_k}}} d\varepsilon_{\hat{N}_k} \quad (48)$$

Figure 5 shows that this probability of wrong fixing is almost constant over time and that it enables a substantial improvement over the traditional approach especially for poor satellite geometries.

The price for extremely reliable ambiguity fixing is an increased combination noise and, thus, a less accurate position estimate compared to uncombined measurements.

However, a reliable fixing of uncombined measurements is not feasible within a few epochs. Therefore, the float solution of uncombined measurements shall be compared with the fixed solution of combined measurements in Figure 6.

One can observe that the latter approach enables a more than two times smaller standard deviation, which indicates that the benefit of fixing more than compensates for the noise amplification by the linear combinations. The positioning accuracies were computed for simulated E1 and E5 double difference measurements of three epochs for a Galileo satellite geometry with 8 visible satellites. The float solution was obtained from a least-squares estimation of uncombined float ambiguities, baselines (once per

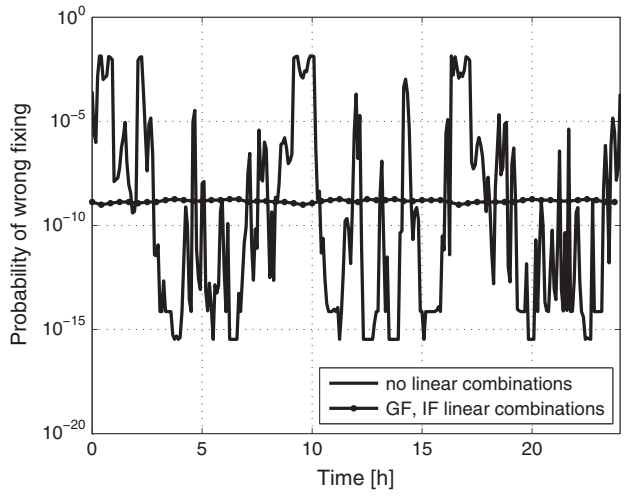

Fig. 5–Benefit of geometry-free, ionosphere-free linear combinations for integer ambiguity resolution

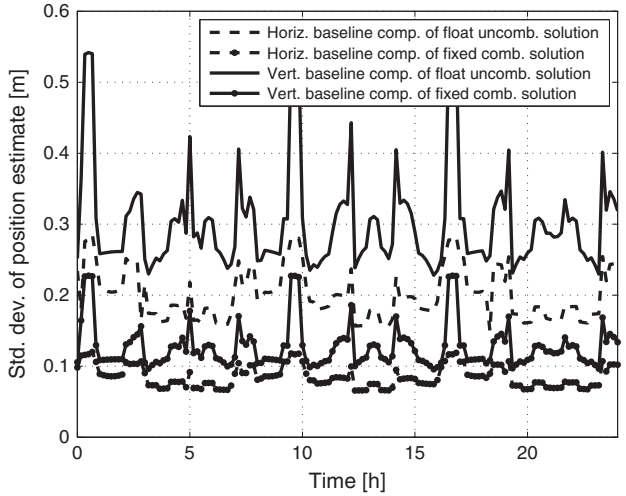

Fig. 6–Comparison between float solution of uncombined measurements and fixed solution of combined measurements: The benefit of fixing more than compensates for the noise amplification by the linear combinations

epoch) and slant double differenced ionospheric delays (once per epoch). The fixed solution was obtained from a least-squares estimation of the baselines (one estimate per epoch).

INTEGER AMBIGUITY RESOLUTION WITH STATISTICAL *A PRIORI* KNOWLEDGE OF ATTITUDE

The linear combinations of the previous section can be used for both absolute (Precise Point Positioning, PPP) and differential (Real Time Kinematics, RTK) positioning. In the latter case, the reliability of integer ambiguity resolution can be further improved by some *a priori* information on the attitude. This *a priori* information can be given either in the form of a fixed/deterministic baseline length, elevation and/or azimuth, or in the form of probability distributions of these spherical baseline parameters. Figure 7 visualizes the wavefronts from three satellites and the respective intersection points, the search space volume spanned by the pure code solution (indicated as circle), and its reduction by constraints on the baseline length and direction. A certain interval has been introduced for both parameters to allow some variations in the *a priori* information.

The constrained integer ambiguity resolution motivates a spherical parameterization of the baseline vector of (35), i.e.,

$$\xi = r(v_1, v_2) \cdot l \tag{49}$$

with elevation v_1, azimuth v_2, baseline length l, and normalized baseline vector

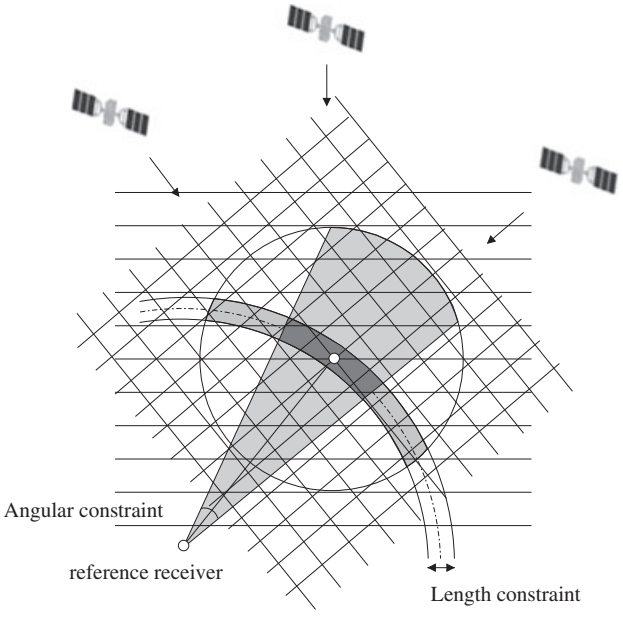

Fig. 7–Integer ambiguity grid: Constraints on the baseline length and direction reduce the search space volume

$$r(v_1, v_2) = \begin{bmatrix} cos(v_1)cos(v_2) \\ cos(v_1)sin(v_2) \\ sin(v_1) \end{bmatrix} \tag{50}$$

The maximum a posteriori probability (MAP) estimates of v_1, v_2 and l are obtained with the rule of Bayes as

$$\begin{aligned} &\max_{v_1,v_2,l} p(v_1, v_2, l|\Psi) \\ &\quad = \max_{v_1,v_2,l} p(\Psi|v_1, v_2, l) \cdot \frac{p(v_1, v_2, l)}{p(\Psi)} \end{aligned} \tag{51}$$

where the first factor is in general modeled as a Gaussian distribution, i.e.,

$$p(\Psi|v_1, v_2, l) = \frac{1}{\sqrt{(2\pi)^k |\Sigma|}} e^{-\frac{1}{2}\|\Psi - Hr(v_1,v_2)l - AN\|^2_{\Sigma^{-1}}} \tag{52}$$

and the second factor represents the *a priori* information.

Baseline *A Priori* Knowledge: Gaussian Distributions

In a large number of applications, *a priori* knowledge about the baseline is available in the form of statistically independent Gaussian distributions with known means $\bar{l}, \bar{v}_x, x \in \{1, 2\}$ and variances $\sigma^2_{\bar{l}}$ and $\sigma^2_{\bar{v}_x}$, i.e.,

$$\begin{aligned} p(v_x) &= \frac{1}{\sqrt{2\pi\sigma^2_{\bar{v}_x}}} e^{-\frac{(v_x - \bar{v}_x)^2}{2\sigma^2_{\bar{v}_x}}}, \quad x \in \{1, 2\} \\ p(l) &= \frac{1}{\sqrt{2\pi\sigma^2_{\bar{l}}}} e^{-\frac{(l-\bar{l})^2}{2\sigma^2_{\bar{l}}}} \end{aligned} \tag{53}$$

The remaining parameter $p(\Psi)$ in (51) is a marginal distribution that is given by

$$p(\Psi) = \int\int\int p(\Psi|v_1, v_2, l) p(v_1) p(v_2) p(l) dv_1 dv_2 dl \tag{54}$$

which corresponds to a normalization. The maximization of (51) can be simplified by taking the logarithm and omitting the pre-factor that does not depend on v_1, v_2 and l:

$$\begin{aligned} &\min_{v_1,v_2,l,N} J(v_1, v_2, l, N) \\ &\quad = \min_{v_1,v_2,l,N} \left(\|\Psi - Hr(v_1, v_2)l - AN\|^2_{\Sigma^{-1}} \right. \\ &\qquad \left. + \frac{(l-\bar{l})^2}{\sigma^2_{\bar{l}}} + \frac{(v_1 - \bar{v}_1)^2}{\sigma^2_{\bar{v}_1}} + \frac{(v_2 - \bar{v}_2)^2}{\sigma^2_{\bar{v}_2}} \right) \end{aligned} \tag{55}$$

This minimization is split into three steps similar to the unconstrained case. First, a classical least-squares float solution is determined by disregarding the *a priori* information and integer nature of ambiguities. Secondly, a tree search is performed to determine all integer candidate vectors inside a pre-defined search space volume. The efficiency of

this search is substantially improved if the number of paths is reduced by inequality constraints on the estimated baseline parameters. The unconstrained search tree is described in details by Teunissen in [16] and the length constrained one by Mönikes et al. in [17], by Teunissen in [18] and [19], and by Giorgi *et al*. in [20]. Jurkowski *et al*. introduced constraints on the baseline direction in [21] to further improve the efficiency of the search, and Henkel et al. integrated a state space model for the baseline length and attitude in a Kalman filter in [22]. The third step includes the constrained baseline determination for each integer candidate vector and, finally, the candidate with smallest weighted range residuals is selected. The third step is solved iteratively with the Newton method, i.e., the baseline parameters are given in the n-th step by

$$\begin{bmatrix} \hat{v}_1^{n+1} \\ \hat{v}_2^{n+1} \\ \hat{l}^{n+1} \end{bmatrix} = \begin{bmatrix} \hat{v}_1^{n} \\ \hat{v}_2^{n} \\ \hat{l}^{n} \end{bmatrix} - S^{-1} \begin{bmatrix} \frac{\partial J}{\partial v_1} \\ \frac{\partial J}{\partial v_2} \\ \frac{\partial J}{\partial l} \end{bmatrix} \tag{56}$$

where $\hat{v}_x$, $x \in \{1, 2\}$, and $\hat{l}$ include the estimates, and the Hesse matrix is given by

$$S = \begin{bmatrix} \frac{\partial^2 J}{\partial v_1^2} & \frac{\partial^2 J}{\partial v_1 \partial v_2} & \frac{\partial^2 J}{\partial v_1 \partial l} \\ \frac{\partial^2 J}{\partial v_1 \partial v_2} & \frac{\partial^2 J}{\partial v_2^2} & \frac{\partial^2 J}{\partial v_2 \partial l} \\ \frac{\partial^2 J}{\partial v_1 \partial l} & \frac{\partial^2 J}{\partial v_2 \partial l} & \frac{\partial^2 J}{\partial l^2} \end{bmatrix} \tag{57}$$

The initial values of the spherical baseline parameters could be obtained by a classical least-squares estimation of the cartesian baseline coordinates, followed by a coordinate transformation.

Figure 8 shows the benefit of a tight and soft length constraint for integer least-squares estimation (ILS) with Galileo. Double difference measurements on E1 and E5 were simulated for a baseline length of 30 m, a geometry with 8 visible satellites, 4 measurement epochs, and a standard deviation of 1 mm for the phase noise. Phase-only measurements were considered to avoid code multipath, and a wide-lane combination with a wavelength of 78.1 cm was chosen to increase the success rate. Obviously, the tightly constrained (TC) ambiguity resolution reduces the probability of wrong unconstrained fixing by more than four orders of magnitude if the *a priori* length information is correct. However, it makes the fixing also sensitive w.r.t. erroneous *a priori* information, i.e. it degrades the unconstrained performance if the error in the *a priori* information exceeds 50 cm. The soft constrained (SC) fixing takes the uncertainty in the length information into account and, thereby, improves the unconstrained fixing for

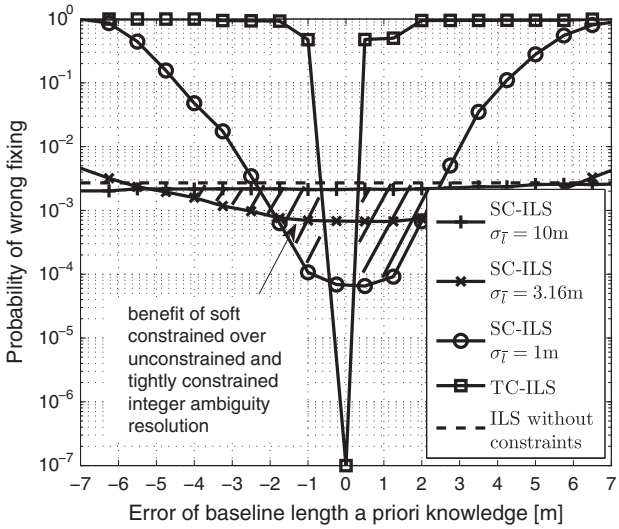

Fig. 8–Comparison of unconstrained, soft constrained and tightly constrained ambiguity resolution for erroneous baseline length a priori information: The tightly constrained ambiguity resolution outperforms the unconstrained and soft constrained fixing for perfect a priori knowledge but is extremely sensitive w.r.t. erroneous a priori information. The soft constrained ambiguity fixing benefits from the a priori information even if it is biased

quality of the *a priori* information. Note that the unconstrained ambiguity resolution is obtained from the SC one by setting $\sigma_{\hat{l}} \to \infty$. The TC ambiguity fixing can also be obtained from Lagrange optimization with an equality constraint (e.g. Teunissen [19]).

Baseline *A Priori* Knowledge: Inequality Constraints

The maximum *a posteriori* probability estimation enables a substantial improvement in ambiguity fixing as it benefits from an *a priori* known Gaussian probability distribution of the baseline parameters. However, if this information is erroneous or unavailable, inequality constraints can be very beneficial. These constraints can be regarded as uniform distributions that do not favor any baseline length or direction. The optimization problem is written as

$$\begin{aligned} \min_{v_1, v_2, l, N \in \mathbb{Z}^{K\times 1}} & \parallel \Psi - Hr(v_1, v_2)l - AN \parallel^2_{\Sigma^{-1}} \\ s.t. & \; v_{1,min} \le v_1 \le v_{1,max}, \\ & \; v_{2,min} \le v_2 \le v_{2,max}, \\ & \; l_{min} \le l \le l_{max} \end{aligned} \tag{58}$$

with l_{min}, $v_{1,min}$, $v_{2,min}$ being lower bounds and l_{max}, $v_{1,max}$, $v_{2,max}$ referring to upper bounds on the spherical baseline parameters. The inequality constrained ambiguity resolution can be approximated by an unconstrained optimization problem as described by Henkel and Zhu in [23], i.e.

$$\begin{aligned} \min_{v_1, v_2, l, N \in \mathbb{Z}^K} & \left(\|\Psi - Hr(v_1, v_2)l - AN\|^2_{\Sigma^{-1}} \right. \\ & \left. + \sum_{i=1}^{2} f(v_i, v_{i,min}, v_{i,max}) + f(l, l_{min}, l_{max}) \right) \end{aligned} \tag{59}$$

with the barrier function

$$f(x, x_{min}, x_{max}) = \begin{cases} t \cdot (x_{min} - x)^h & x < x_{min} \\ 0 & x_{min} \le x \le x_{max} \\ t \cdot (x - x_{max})^h & x > x_{max} \end{cases} \quad (60)$$

with penalty factor t and $h \ge 3$. This barrier function is second order continuously differentiable so that the minimization of (59) can be again solved iteratively with the Newton method. For $t \to \infty$, (59) is equivalent to (58).

SUCCESS RATE DETERMINATION FOR ROUNDING OF FLOAT SOLUTION

Simple rounding of the float solution has recently received little attention mainly for two reasons. First, it provides a lower success rate than sequential bootstrapping and integer least-squares estimation for unbiased measurements. Secondly, there does not exist a closed-form expression for the evaluation of the success rate of rounding. Therefore, the easily computable success rate of bootstrapping became the defacto standard, either used as a lower bound for integer least-squares estimation or directly used to characterize bootstrapping.

However, the simple rounding could be an interesting candidate for precise point positioning as it is less sensitive with respect to unknown biases than sequential ambiguity fixing and integer least-squares estimation. The sequential estimation accumulates the biases of various satellites, the integer decorrelation might cancel or amplify them (depending on the signs and magnitudes of the unknown biases and combination coefficients), and the search might additionally reduce the success rate due to the negligence of biases. The simple rounding prevents these risks. Consequently, there is a need for an efficient computation of the success rate of rounding as Monte-Carlo simulations are practically unacceptable for error rates in the order of magnitude of 10^{-9}. Genz suggested in [24] an efficient method for the evaluation of the multivariate cumulative normal distribution. This method uses three integral transformations [22] and shall be applied for the evaluation of the success rate, which is given by

$$P_s = P\left(\left[\hat{N}\right] = N\right) = \frac{1}{\sqrt{\left|\Sigma_{\hat{N}}\right|(2\pi)^K}} \cdot \int_{-0.5-b_1}^{+0.5-b_1} \dots \int_{-0.5-b_K}^{+0.5-b_K} e^{-\frac{1}{2}\varepsilon_{\hat{N}}^T \Sigma_{\hat{N}}^{-1} \varepsilon_{\hat{N}}} \, d\varepsilon_{\hat{N}_1} \dots d\varepsilon_{\hat{N}_K} \quad (61)$$

where $\varepsilon_{\hat{N}} = \hat{N} - N$ denotes the error of the float solution $\hat{N}$. It is normal distributed, i.e.

$$\varepsilon_{\hat{N}} \sim \mathcal{N}\left(0, \Sigma_{\hat{N}}\right) \quad (62)$$

with the float ambiguity covariance matrix $\Sigma_{\hat{N}}$. The Choleskey decomposition is used to diagonalize the error vector, i.e.

$$e_{\hat{N}} = C^{-1} \varepsilon_{\hat{N}} \quad (63)$$

with

$$\Sigma_{\hat{N}} = CC^T \quad (64)$$

Thus, the success rate of (61) can be rewritten as

$$P_s = \frac{1}{\sqrt{(2\pi)^K}} \int_{l_1}^{u_1} e^{-\frac{e_{\hat{N}_1}^2}{2}} \int_{l_2\left(e_{\hat{N}_1}\right)}^{u_2\left(e_{\hat{N}_1}\right)} e^{-\frac{e_{\hat{N}_2}^2}{2}} \dots \cdot \int_{l_K\left(e_{\hat{N}_1}, \dots, e_{\hat{N}_{K-1}}\right)}^{u_K\left(e_{\hat{N}_1}, \dots, e_{\hat{N}_{K-1}}\right)} e^{-\frac{e_{\hat{N}_K}^2}{2}} de_{\hat{N}_1} de_{\hat{N}_2} \dots de_{\hat{N}_{K-1}} \quad (65)$$

where the correlation between the float ambiguities is included in the integration limits l_k and u_k. These limits are obtained from the inequalities

$$-0.5 - b_k \le \varepsilon_{\hat{N}_k} = \sum_{j=1}^{k} C_{kj} e_{\hat{N}_j} \le +0.5 - b_k \quad (66)$$

which can be solved for $e_{\hat{N}_k}$:

$$l_k \le e_{\hat{N}_k} \le u_k \quad (67)$$

with

$$l_k = \frac{-0.5 - b_k - \sum_{j=1}^{k-1} C_{kj} e_{\hat{N}_j}}{C_{kk}}$$
$$u_k = \frac{+0.5 - b_k - \sum_{j=1}^{k-1} C_{kj} e_{\hat{N}_j}}{C_{kk}} \quad (68)$$

The second transformation uses the cumulative normal distribution to absorb the exponential functions of (65), i.e.

$$z_k = \Phi\left(e_{\hat{N}_k}\right) \quad (69)$$

with

$$\Phi(v) = \frac{1}{\sqrt{2\pi}} \int_{-\infty}^{v} e^{-\frac{1}{2}\theta^2} d\theta \quad (70)$$

Thus, (65) simplifies to

$$P_s = \int_{l'_1}^{u'_1} \int_{l'_2(z_1)}^{u'_2(z_1)} \dots \int_{l'_K(z_1, \dots, z_{K-1})}^{u'_K(z_1, \dots, z_{K-1})} dz_1 dz_2 \dots dz_K \quad (71)$$

with the transformed integration limits

$$l'_k = \Phi\left(\frac{1}{C_{kk}}\left(-0.5 - b_k - \sum_{j=1}^{k-1} C_{kj} \Phi^{-1}(z_j)\right)\right)$$
$$u'_k = \Phi\left(\frac{1}{C_{kk}}\left(+0.5 - b_k - \sum_{j=1}^{k-1} C_{kj} \Phi^{-1}(z_j)\right)\right)$$

Finally, Genz's third transformation is given by

$$w_k = \frac{z_k - l'_k}{u'_k - l'_k} \tag{72}$$

which puts the integral into a constant limit form, i.e.,

$$\begin{aligned} P_s = (u'_1 - l'_1) \int_0^1 (u'_2 - l'_2) \int_0^1 \dots \\ (u'_K - l'_K) \int_0^1 dw_1 dw_2 \dots dw_K \end{aligned} \tag{73}$$

Eq. (73) can be expanded to

$$\begin{aligned} P_s = (u'_1 - l'_1) \int_0^1 (u'_2 - l'_2) f(w_1) \int_0^1 \dots \\ (u'_K - l'_K) f(w_{K-1}) \int_0^1 f(w_K) dw_1 \dots dw_K \end{aligned} \tag{74}$$

with

$$f(w_k) = \begin{cases} 1 & \text{if} \quad 0 \le w_k \le 1 \\ 0 & \text{else} \end{cases} \tag{75}$$

The introduction of $f(w_k)$ does not change the value of P_s but it allows us to interpret w_k as a uniformly distributed random variable between 0 and 1. Thus, (74) can also be written as

$$P_s = E_{w_1,\dots,w_K} \left\{ \prod_{k=1}^{K} \left(u'_k(w_1, \dots, w_K) - l'_k(w_1, \dots, w_K) \right) \right\} \tag{76}$$

with $w_k \sim \mathcal{U}(0,1)$ for all k. The success rate of (76) can be efficiently computed using Monte-Carlo simulation or more advanced numerical integration techniques, e.g. the subregion adaptive method as discussed by Genz in [24].

Figure 9 shows the benefit of computing the expectation value w.r.t. w_k in (76) instead of w.r.t. $\varepsilon_{\hat{N}}$ in (61). The computational burden is measured by the time required to estimate P_s with a dual core 2.1 GHz CPU. The use of the three integral transformations enables a substantial reduction in computation time. A realtime evaluation becomes feasible.

Figure 10 shows the probability of wrong fixing for various integer estimation techniques. An

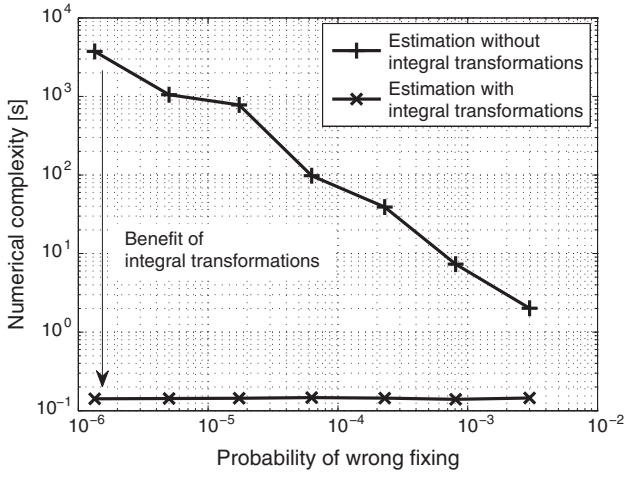

Fig. 9–Efficient computation of success rate of rounding with integral transformations

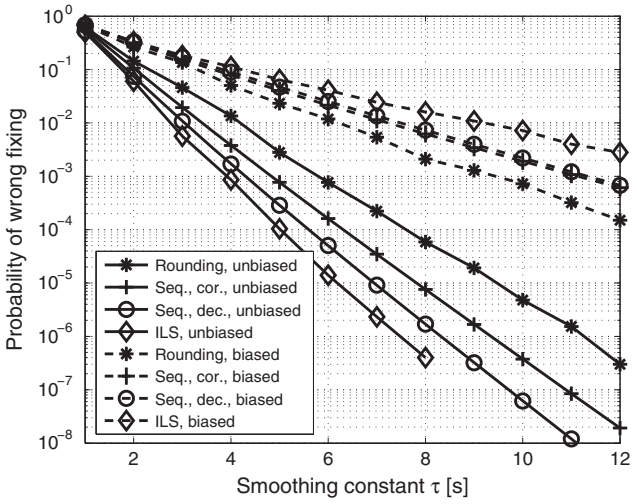

Fig. 10–Comparison of various integer ambiguity resolution techniques for both unbiased and biased measurements with worst-case accumulation of biases

ionosphere-free carrier smoothing is applied to two GP-IF linear combinations (a code carrier combination of maximum discrimination and a code-only combination) of E1 and E5 measurements to improve the reliability of widelane ambiguity resolution. Obviously, a larger smoothing period results in a lower error rate. For unbiased measurements, the integer least-squares estimation achieves the lowest error rate of all fixing methods. A slightly higher error rate can be observed for sequential fixing with integer decorrelation due to the lack of an integer search. An additional degradation occurs if the integer decorrelation is omitted, and the largest error rate is obtained for rounding as it does not consider the correlations between the float ambiguity estimates. The success rate of rounding is computed with (76).

The ranking of the fixing techniques might completely change in the presence of multiple biases, e.g. due to multipath. In this case, the conditioning of float ambiguity estimates on other ambiguities as well as the application of an ambiguity transformation lead to an accumulation of biases, which might cancel but might also be substantially amplified depending on the signs of the combination coefficients and unknown biases. For the simulation results shown in Figure 10, a worst-case bias accumulation was considered. The magnitudes were chosen from an elevation dependent exponential profile, and set to 1 cm for pseudorange measurements of satellites being in the zenith and to 10 cm for satellites being in the horizon. For the phase multipath, 0.01 cycles and 0.1 cylces were assumed respectively. In this case, rounding achieves the lowest error rate, followed by sequential fixing without and with integer decorrelation. The integer decorrelation amplifies the biases and the search criterion is suboptimal which results in the largest error rate. Consequently, the most simple method is also the most robust one: the rounding of the float solution.

CONCLUSION

In this paper, two methods were suggested to improve the reliability of carrier phase integer ambiguity resolution for Real-Time Kinematics (RTK) and Precise Point Positioning (PPP). The first one was a new group of linear combinations that include both code and carrier phase measurements on two or more frequencies. An arbitrary scaling of the geometry, an arbitrary scaling of the ionospheric delay, and any preferred wavelength can be obtained with these linear combinations. The maximization of the ambiguity discrimination leads to combinations with a wavelength of several meters and a noise level of a few centimeters. The integer ambiguities of these combinations can be resolved with a probability of wrong fixing of less than 10^{-9} with measurements from a few epochs. These combinations are recommended for any application where reliability is more important than accuracy. The second method incorporated some statistical attitude *a priori* knowledge into the ambiguity fixing. The *a priori* information included both the baseline length and orientation, and is typically given either as Gaussian or uniform distributions. It enables a substantial reduction of the integer search space volume but also ensures a large robustness over errors in the *a priori* information. Both the multi-frequency code carrier linear combinations and the soft baseline constraints improve the float ambiguity estimates, such that a simple rounding achieves reliable integer estimates.

In the last part of this article, an efficient method for the computation of the success rate of rounding was proposed to avoid the currently used inaccurate bounds or extensive Monte-Carlo simulations. The suggested method is based on a transformation of the cumulative multivariate Gaussian distribution into cumulative uniform distributions, which can be efficiently evaluated in realtime.

REFERENCES

1. Blewitt, G., "Carrier-Phase Ambiguity Resolution for the Global Positioning System Applied to Geodetic Baselines up to 2000 km," *Journal of Geophysical Research*, Vol. 94, No. B8, 1989, pp. 10.187–10.203.
2. Teunissen, P., "Integer Estimation in the Presence of Biases," *Journal of Geodesy*, 2001, pp. 399–407.
3. Cocard, M. and Geiger, A., "Systematic Search for All Possible Widelanes," *Proceedings of the 6th International Geodetic Symposium on Satellite Positioning*, Ohio, 1992, pp. 312–318.
4. Collins, P., "An Overview of GPA Inter-Frequency Carrier Phase Combinations," *Technical Memoranda*, Geodetic Survey Division, University of New Brunswick, Canada, 1999, pp. 1–15.
5. Henkel, P. and Günther, C., "Three Frequency Linear Combinations for Galileo," *Proceedings of the 4th IEEE Workshop on Position, Navigation, and Communication (WPNC)*, Hannover, Germany, March 2007, pp. 239–245.
6. Wübbena, G., "New GNSS Signals and Ambiguity Resolution," *Proceedings of EGU General Assembly*, Vienna, Austria, 2007.
7. Richert, T. and El-Sheimy, N., "Optimal Linear Combinations of Triple Frequency Carrier Phase Data from Future Global Navigation Satellite Systems," *GPS Solutions*, Vol. 11, 2007, pp. 11–19.
8. Henkel, P. and Günther, C., "Joint L-/C-Band Code and Carrier Phase Linear Combinations for Galileo," *International Journal of Navigation and Observation*, Vol. 2008, Article ID 651437, 2008.
9. Henkel, P., Gomez, V. and Günther, C., "Modified LAMBDA for Absolute Carrier Phase Positioning in the Presence of Biases," *Proceedings of the 2009 International Technical Meeting of The Institute of Navigation*, Anaheim, CA, January 2009, pp. 642–651.
10. Henkel, P., "Bootstrapping with Multi-Frequency Mixed Code Carrier Linear Combinations and Partial Integer Decorrelation in the Presence of Biases," *Proceedings of the International Association of Geodetic Scientists Association*, Buenos Aires, Argentina, 2009, pp. 923–931.
11. Henkel, P. and Günther, C., "Reliable Integer Ambiguity Resolution with Multi-Frequency Code Carrier Linear Combinations," *Proceedings of the 23rd International Technical Meeting of The Satellite Division of The Institute of Navigation (ION GNSS 2010)*, Portland, OR, September 2010, pp. 185–195.
12. Henkel, P. and Günther, C., "Reliable Integer Ambiguity Resolution with Multi-Frequency Code Carrier Linear Combinations," *GPS World*, 2010.
13. Henkel, P. and Günther, C., "Reliable Integer Ambiguity Resolution with Multi-Frequency Code Carrier Linear Combinations," *Journal of Global Positioning Systems*, Vol. 9, No. 2, 2010, pp. 90–103.
14. Betz, J., "Binary Offset Carrier Modulations for Radio-Navigation," *NAVIGATION*, Vol. 48, No. 4, 2002, pp. 227–246.
15. Teunissen, P., "An Optimality Property of the Integer Least-Squares Estimator," *Journal of Geodesy*, Vol. 70, 1995, pp. 65–82.
16. Teunissen, P., "The Least-Squares Ambiguity Decorrelation Adjustment: A Method for Fast GPS Ambiguity Estimation," *Journal of Geodesy*, Vol. 73, 1999, pp. 587–593.
17. Monikes, R., Wendel, J. and Trommer, G. F., "A Modified Lambda Method for Ambiguity Resolution in the Presence of Position Domain Constraints," *Proceedings of the 18th International Technical Meeting of the Satellite Division of The Institute of Navigation (ION GNSS 2005)*, Long Beach, CA, September 2005, pp. 81–87.
18. Teunissen, P., "The LAMBDA Method for the GNSS Compass," *Artificial Satellites*, Vol. 41, No. 3, 2006, pp. 89–103.
19. Teunissen, P., "Integer Least-Squares Theory for the GNSS Compass," *Journal of Geodesy*, Vol. 84, 2010, pp. 433–447.

20. Giorgi, G., Teunissen, P., and Buist, P., "A Search and Shrink Approach for the Baseline Constrained LAMBDA Method: Experimental Results," *Proceedings of the International Symposium on GPS/GNSS*, Tokyo University of Marine Science and Technology, 2008, pp. 797–806.
21. Jurkowski, P., Henkel, P., Gao, G. X., and Günther, C., "Integer Ambiguity Resolution with Tight and Soft Baseline Constraints for Freight Stabilization at Helicopters and Cranes," *Proceedings of the 2011 International Technical Meeting of The Institute of Navigation*, San Diego, CA, January 2011, pp. 336–346.
22. Henkel, P., Jurkowski, P. and Günther, C., "Differential Integer Ambiguity Resolution with Gaussian *a Priori* Knowledge and Kalman Filtering," *Proceedings of the 24th International Technical Meeting of The Satellite Division of The Institute of Navigation (ION GNSS 2011)*, Portland, OR, September 2011, pp. 3881–3888.
23. Henkel, P. and Zhu, C., "Phase Integer Ambiguity Resolution with Inequality Constraints for GPS and Galileo," *Proceedings of the IEEE Statistical Signal Processing Workshop*, Nice, France, 2011, pp. 409–412.
24. Genz, A., "Numerical Computations of Multivariate Normal Probabilities," *Journal of Computational and Graphical Statistics*, 1992, pp. 141–149.
25. Henkel, P., Reliable Carrier Phase Positioning, Ph. D. Thesis, Technische Universitat Munchen, Verlag Dr. Hut, ISBN 978-3-86853-716-1, 2010.